Estonian Journal of Earth Sciences
2023, **72**, 2, 185–196

https://doi.org/10.3176/earth.2023.84

www.eap.ee/earthsciences
Estonian Academy Publishers

RESEARCH ARTICLE

Received 25 November 2022
Accepted 21 February 2023
Available online 22 October 2023

Keywords:
electrical resistivity tomography, 3D modelling, shallow subsurface, gypsum karst, Latvia

Corresponding author:
Jānis Karušs
janis.karuss@lu.lv

Citation:
Karušs, J., Džeriņš, P., Lamsters, K., Ješkins, J. and Stinkulis, Ģ. 2023. Limitations in detectability of air-filled gypsum karst cavity by electrical resistivity tomography; a case study from the Baltic Devonian sedimentary basin. *Estonian Journal of Earth Sciences*, **72**(2), 185–196. https://doi.org/10.3176/earth.2023.84

Limitations in detectability of air-filled gypsum karst cavity by electrical resistivity tomography: a case study from the Baltic Devonian sedimentary basin

Jānis Karušs, Pēteris Džeriņš, Kristaps Lamsters, Jurijs Ješkins and Ģirts Stinkulis

Faculty of Geography and Earth Sciences, University of Latvia, Jelgavas iela 1, Riga, LV-1004, Latvia

ABSTRACT

Karst terrain is widely distributed globally, posing one of the most significant issues for civil engineering and public safety. Electrical resistivity tomography (ERT) is regarded as the most suitable method for exploring subsurface karst features. Nevertheless, ambiguities in the ERT inversion process can arise due to specific geological conditions. In this study, we used measurements obtained in the area next to a recently developed gypsum karst sinkhole in Latvia and 3D geophysical modelling to specifically analyse the limitations in identifying near-surface air-filled karst voids by ERT. Our results emphasise that due to the 3D effect, even the recent sinkhole may be undetectable in ERT data, despite the placement of ERT profiles directly above the overhanging part of the 7-m-deep sinkhole. The 2D synthetic modelling results suggest that a karst sinkhole of similar size to the one surveyed in the field should be easily recognised. In contrast, the results obtained with 3D synthetic modelling reveal almost no indication of a sinkhole in the modelled profiles. We conclude that 2D synthetic modelling cannot always be used to assess the possibilities of identifying subsurface cavities with the ERT method. Reliable assessment can only be achieved using 3D synthetic modelling techniques. Our results demonstrate that problems with detecting air-filled karst sinkholes can arise not only in areas where surrounding rocks have a high electrical resistivity but also where surrounding rocks have a low resistivity.

Introduction

Karst is a terrain with distinctive hydrogeology and landforms that arise from high rock solubility and well-developed secondary porosity (Ford and Williams 2007; Gutiérrez et al. 2014). Karst terrain forms via dissolution of rocks by acidic waters infiltrating into them. Typical causes of water acidity are atmospheric CO_2 that dissolves in water and organic acids or oxidation processes occurring in oxygen-rich conditions (Gutiérrez et al. 2014). As karst terrain is widely distributed across the continents, including densely populated areas, it poses a significant issue for civil engineering and public safety (Martel et al. 2018). Environmental problems associated with karst and groundwater abstraction and agriculture are also essential in the Baltic countries, including Latvia (Paukstys and Narbutas 1996; Levins and Buzajevs 1999).

In most cases, carbonate rocks are exposed to karst processes, but karst develops more rapidly in the areas where highly soluble rocks such as gypsum and halite are found (Gutiérrez et al. 2014). Gypsum has a high solubility (2.4 g/L in water at 20 °C), with a dissolution rate of up to 100 times higher than that of carbonate rocks. Thus, karst in gypsum rocks evolves much faster and can cause severe problems to infrastructure (Pando et al. 2013; Gutiérrez et al. 2014; Drahor 2019; Gökkaya et al. 2021). Despite the foregoing, gypsum karst has received limited attention compared with limestone karst, resulting in a lesser degree of determined ambiguities in its exploration (Gutiérrez et al. 2008; Gökkaya et al. 2021).

Various methods are used to explore karst (for a review, see Gutiérrez et al. 2014). Direct investigation methods such as drillings, excavations, etc., provide only point-wise information about the subsurface, contrary to geophysical methods, which allow

us to obtain nearly continuous data coverage over the study area. In many cases, geophysical survey methods are applied to locate various karst features, especially karst voids and caves, which are characterised by high contrast within host rocks in terms of electrical resistivity, density, and seismic properties (Zhou et al. 2002; Chalikakis et al. 2011; Gutiérrez et al. 2014; Martínez-Moreno et al. 2014; Martel et al. 2018; Rao et al. 2021). Nonetheless, as Chalikakis et al. (2011) highlighted, geophysical methods are not systematically used for karst-system exploration, and the possibility of detecting underground cavities needs further study.

Some authors (Satitpittakul et al. 2013; Drahor 2019) argue that due to the relatively simple data-gathering process and superior capabilities of characterising karst geometries, physical contrasts, dissolution zones and sedimentary units of collapsed sections, electrical resistivity tomography (ERT) is the most suitable method. Nevertheless, ERT measurements are indirect, and ambiguities in the inversion process can arise due to specific geological conditions.

Typically, anomalies of very high electric resistivity in karst terrains are interpreted as voids because air has a much higher resistivity than surrounding rocks. Nonetheless, resistivity variations across a gypsum karst formation can be erratic due to the complex gypsum karstification character. Consequently, interpreting the obtained resistivity data is not straightforward (Drahor 2019). Even a poor contact between electrodes and the ground surface can create a high resistivity artefact during the data inversion process (Satitpittakul et al. 2013). Researchers usually try to overcome such ambiguities using multiple geophysical methods (for a review, see Martínez-Moreno et al. 2014). For example, the inversion model obtained by the ERT method can be significantly improved if some constraints are applied to the model (Loke 2004; Karušs et al. 2021; Džeriņš et al. 2023). Nonetheless, such an approach increases substantially the cost of the survey, and as a result, is not commonly applied.

In this study, we focus on the limitations of identifying near-surface air-filled karst voids using ERT. Only a few studies have addressed this question, most of which are devoted to geophysical modelling (Satitpittakul et al. 2013). We used the measurements obtained in the area next to the recently developed karst sinkhole and geophysical modelling, which allowed us to test the detection capabilities of karst voids and sinkholes by various ERT settings and configurations.

Study area

The study area lies in central Latvia (Fig. 1), one of the few cover-karst areas in Latvia associated with gypsum bedrock (Paukstys and Narbutas 1996; Levins and Buzajevs 1999). The superficial karst terrain consists mainly of closed depressions such as collapse sinkholes (dolines). Soluble gypsum rocks are overlain by Quaternary sediments, mainly composed of glacial sands and till, the thickness of which in the study area is usually <10 m (Fig. 2) and reaches only up to 4 m near the recently developed sinkhole investigated in this study. The modern topography around the study area has

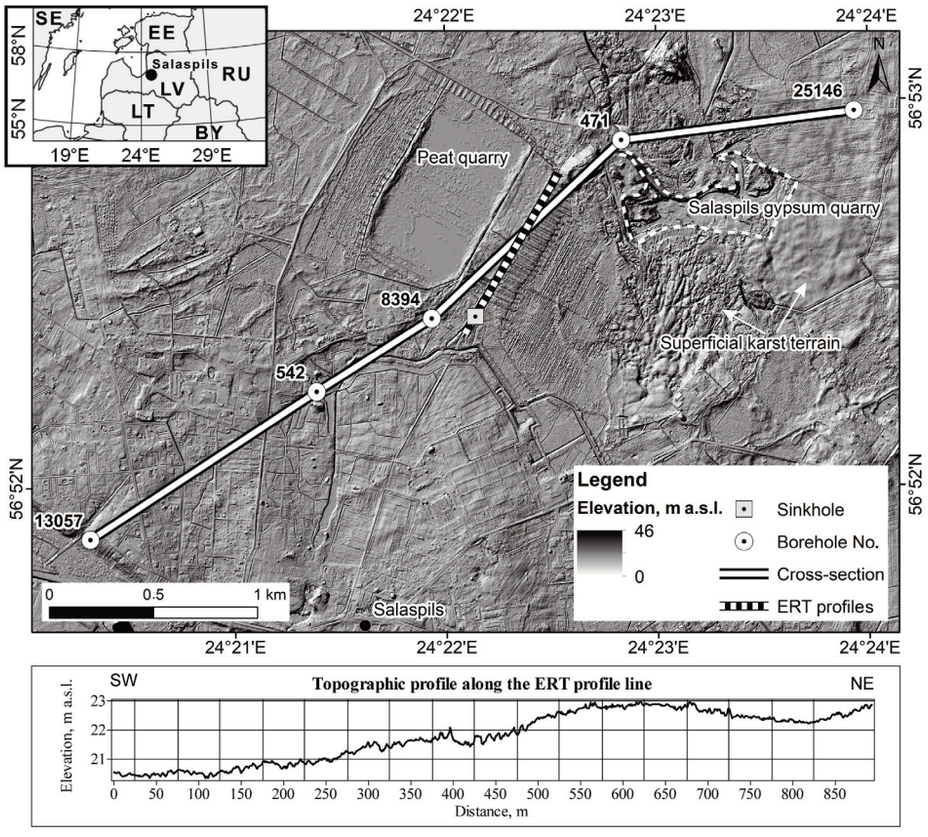

Fig. 1. Location of the ERT profiles with a spacing of 2 and 5 m between electrodes, geological cross-section (Fig. 2B), sinkhole and Salaspils gypsum quarry. LiDAR DEM (Digital Elevation Model) (1 m resolution) is in the background. Note the main superficial karst terrain around the gypsum quarry.

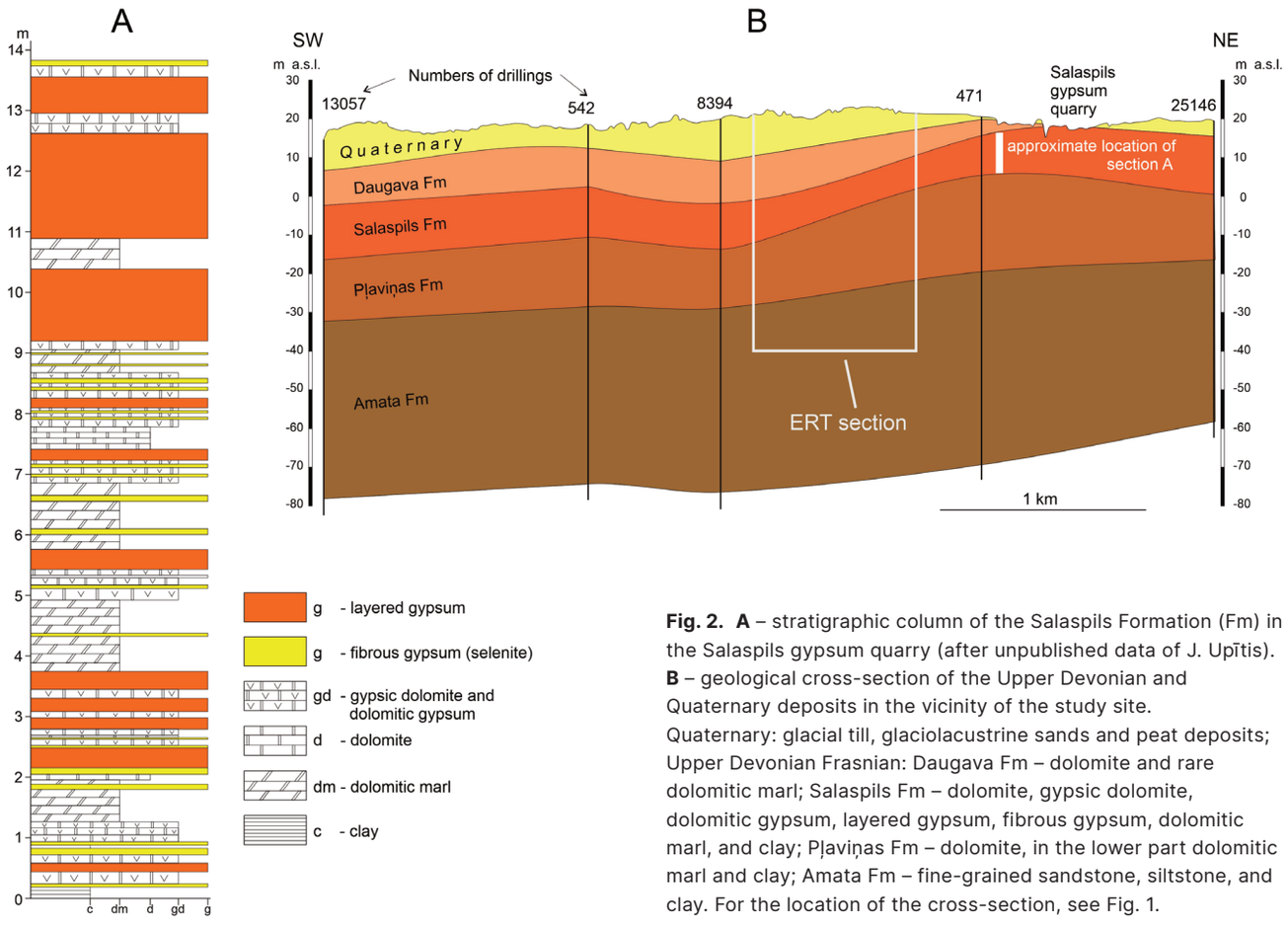

Fig. 2. **A** – stratigraphic column of the Salaspils Formation (Fm) in the Salaspils gypsum quarry (after unpublished data of J. Upītis). **B** – geological cross-section of the Upper Devonian and Quaternary deposits in the vicinity of the study site. Quaternary: glacial till, glaciolacustrine sands and peat deposits; Upper Devonian Frasnian: Daugava Fm – dolomite and rare dolomitic marl; Salaspils Fm – dolomite, gypsic dolomite, dolomitic gypsum, layered gypsum, fibrous gypsum, dolomitic marl, and clay; Pļaviņas Fm – dolomite, in the lower part dolomitic marl and clay; Amata Fm – fine-grained sandstone, siltstone, and clay. For the location of the cross-section, see Fig. 1.

been formed by several glacial advances, with the predominantly erosional activity of the Riga Ice Stream and Zemgale Ice Lobe (Lamsters 2012; Lamsters and Zelčs 2015). Thus, Quaternary sediments are mainly of Early and Late Weichselian age (Lamsters and Zelčs 2015; Lamsters et al. 2017).

The study area corresponds to the NW part of the East European platform, where the Proterozoic basement lies at a depth of ~1000 m (Ivanova and Nulle 2002). Cambrian to Devonian unmetamorphosed sedimentary rocks cover the basement. The upper part of the sub-Quaternary bedrock is represented by the Upper Devonian Daugava Formation (Fm), composed of dolomite with minor dolomitic marl and clay (Fig. 2). In the study area, the Daugava Fm is only 4–10 m thick and dominated by quite highly fissured and water-permeable dolomite. The Daugava Fm is missing, and the rocks of the underlying Salaspils Fm are exposed almost at the ground surface at the nearby Salaspils gypsum quarry (Figs 1 and 2A). The Salaspils Fm is 10–15 m thick (Brangulis et al. 1998) and is typically composed of various alternating layers, such as dolomites, dolomitic marls, and clays, alternated with laminated gypsum, fibrous gypsum, gypsic dolomites and dolomitic gypsum. Mostly layered or laminated, gypsum accounts for ~50% of the section; dolomitic gypsum and gypsic dolomite 25%; and dolomite, dolomitic marl, and clay, in places also with inclusions of gypsum, ~25% (Fig. 2A).

Our survey focuses on the area near the recently developed karst sinkhole, which is situated 900 m SW of the Salaspils gypsum quarry (Fig. 1). There, the average content of $CaSO_4 \cdot 2H_2O$ in the commercial bed of the Salaspils Fm is 87.4% (Kuršs and Stinkule 1997). Therefore, a high content of gypsum is also expected for our study area. Almost the entire thickness of the geological section of the Salaspils Fm embeds in the Salaspils gypsum quarry (Fig. 2B). The high content of gypsum in the Salaspils Fm defines its high solubility and consequential susceptibility to karst processes. Up to 5-m-thick and laterally extensive voids have commonly been encountered during gypsum extraction in the Salaspils quarry. In the eastern part of our study area, subsurface voids reaching a diameter of 12 m have also been reported (Tolstovs et al. 1991). Furthermore, contemporary gypsum dissolution is observable in the quarry (Fig. 3), which may be facilitated by a persistent influx of groundwater due to the substantially lowered groundwater table in the quarry for gypsum extraction purposes.

Methods

Photogrammetric survey of the sinkhole

Insights into the sinkhole morphology and geological structure were obtained from the 3D model. A photogrammetric approach was used to create a digital 3D representation of the sinkhole. A GoPro Hero8 action camera was attached to a long pole and put into the sinkhole on 21.04.2021. During the descent of the camera, the pole was rotated 360° around its axis, and a video was recorded. Light projectors illuminated the lowest part of the sinkhole. This procedure was repeated

Fig. 3. **A**, **B** – studied sinkhole on 21.04.2021. **C** – array of the ERT profile near the sinkhole. **D** – sinkhole after one year on 12.05.2022. Note that after a year, the entire overhanging cover of the sinkhole where the ERT profiles were located has collapsed, and the sinkhole is almost as wide as the road.

several times to achieve full video coverage of all sinkhole parts. Four ground control points (GCPs) were placed around the sinkhole for georeferencing purposes and measured in real-time kinematic (RTK) mode with an Emlid Reach RS2 GNSS receiver. Additional pictures were taken of the scale bar placed near the sinkhole, the GCPs and the entrance.

Afterwards, individual frames were extracted from the 4K video record at 1 s intervals. All dark and blurred frames were rejected since it would be hard to align them, and as a result, they would induce additional sources of errors. The total amount of aligned frames was 903. The photogrammetric processing was carried out in Agisoft Metashape 1.7 software. The workflow for the 3D reconstruction procedure was in accordance with the Agisoft (2021) manual, using the highest quality for the photo alignment, medium quality for building the dense cloud and mild depth filtering. The model result was exported in Wavefront Object file format and measurements of the sinkhole dimensions were obtained in CloudCompare software. The measurements were carried out by bisecting the model in several places.

Electrical resistivity tomography survey

The ERT survey was performed between 20.04.2021 and 30.05.2021 – three weeks after the formation of the sinkhole (29.03.2021). The weather during the data acquisition was mostly sunny, and the ground surface was dry. The average air temperature during the day was approximately 11 °C, and the total precipitation for these 41 days was 109 mm (LEGMC 2021). During the survey, a multi-channel device Syscal Pro Switch (IRIS Instruments) with 72 available stainless steel electrodes was used. Measurements were performed using the Wenner and dipole-dipole electrode configurations (Reynolds 1997). Spacing between the electrodes was set to 1 m and 2 m for a detailed survey of the shallow layers. Five-metre spacing was used for the overall characterisation of the geological cross-section. During acquisition, 400 V was applied to current electrodes; stacking was set to 4, and the duration for each injection was set to 1 s. For the Wenner configuration, 23 depth levels were determined, while for the dipole-dipole configuration, 69 depth levels were determined. Altogether, an over 880-m-long profile with 5 m spacing and a 176-m-long profile with 2 m spacing (Fig. 1) were recorded using a roll-along technique (Geotomo Software 2017; Lamsters et al. 2022). The overlap of the individual profiles was chosen to obtain continuous data coverage down to the depths of approximately 25 m for 2 m electrode spacing (36 electrodes – 72 m overlap) and 50 m for 5 m electrode spacing (36 electrodes – 180 m overlap). Additionally, a 72-m-long ERT profile with 1 m electrode spacing was recorded next to the sinkhole.

The ERT profiles were placed directly above the overhanging part of the sinkhole, which collapsed later in the year,

revealing vertical walls of the sinkhole. The location of the profiles was determined with an RTK GNSS receiver Emlid Reach RS2.

ERT data processing was carried out using RES2DINV software. The first step of data processing was to manually check for any outliers in resistivity values (Loke 2004). In each of the obtained recordings, no more than a few outliers were found. The least-squares inversion of apparent resistivity data was carried out using the quasi-Newton method (Loke and Barker 1996). For the inversion process, the finite-element mesh was used. The model refinement option, which uses model cells with widths of half the electrode spacing, was applied to obtain smoother results. During the inversion process, the L_2 norm (Loke 2004) was used, and the effects of side blocks were reduced severely. The RMS values of the final models were: 2.85% for Wenner 5 m spacing, 3.85% for Wenner 2 m spacing, 8.45% for dipole-dipole 2 m spacing and 0.62% for Wenner 1 m spacing. In all cases, the final model was acquired after seven iterations.

Synthetic modelling

To assess the possibilities of ERT in detecting air-filled underground cavities near the ground surface, we performed synthetic ERT data modelling by RES2DMOD and RES3DMOD software. By using the shape of the sinkhole and underground cavity obtained with the photogrammetric survey as well as the results of the ERT survey, we constructed a conceptual cross-section of the surveyed area. During modelling, a cross-section consisting of two layers was created. The thickness of the upper layer of the glacial till was set to 5 m and its corresponding resistivity to 30 Ohm.m. The resistivity of the lower clay-rich carbonate layer was set to 70 Ohm.m. In contrast, the resistivity of the air-filled cavity placed directly below the Earth's surface was set to 99 999 Ohm.m, representing virtually non-conducting air. The resistivities of both layers and the thickness of the upper layer were determined using ERT field results. The size and shape of the cavity were formed by means of the cavity 3D model obtained via photogrammetry. The height of the cavity was 6 m, and the width 2.5 m.

The results obtained during 3D modelling were used to assess the influence of the 3D effect on the identification of underground cavity near the ground surface. All modelling steps were conducted according to the suggestions of Loke (2004). Later, inversion of the modelled synthetic data was conducted by RES2DINV software.

Results

3D model of the karst sinkhole

A textured 3D sinkhole model was obtained during the photogrammetric process (Fig. 4). Three major lithological units can be distinguished in the model. A technogenic layer embeds at the top, covering a thin layer of buried soil. The soil layer is underlain by Quaternary deposits reaching a thickness of 3.5 m and consisting of glacial till and sandy sediments beneath. A visual inspection revealed that the lower part of the exposed sinkhole comprises a dolomite layer with

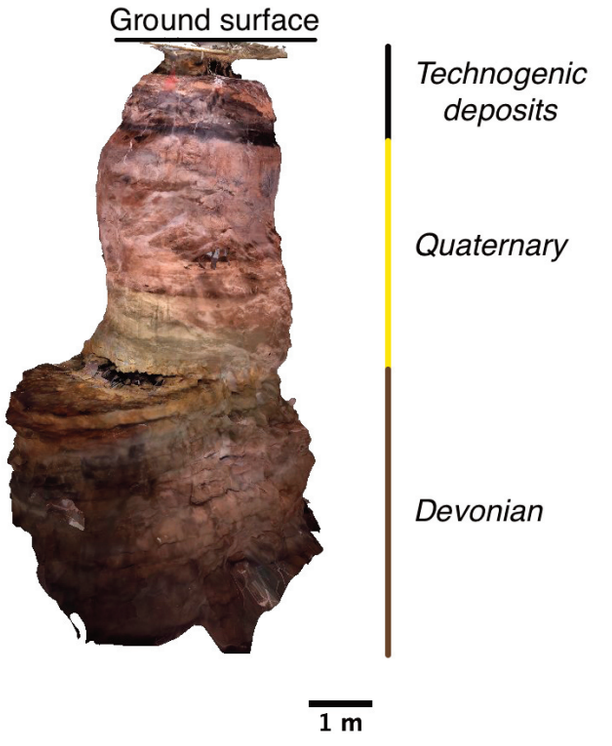

Fig. 4. 3D model of the newly developed karst sinkhole. See the location in Fig. 1.

thin clay and dolomitic marl interlayers. We interpret this layer as the Daugava Fm according to local stratigraphy (Figs 1 and 2), as such thick dolomite layers have not been observed in the Salaspils Fm in the nearby boreholes (Figs 1 and 2). The visible part of the sinkhole is wider in the lower part and resembles a chamber under the upper layer (slab) of dolomite. Prominent irregular surfaces can be seen on the hyporelief at the base of this dolomite layer. These surfaces are probably influenced by dissolution (karst) processes. The floor of the exposed sinkhole is covered by the debris that collapsed from the upper layers, forming a cone in the centre of the sinkhole. This debris-filled part of the sinkhole is mainly formed in the gypsum rocks of the Salaspils Fm, which are exposed in the nearby boreholes and at the Salaspils quarry (Figs 1 and 2).

The sinkhole in its deepest part seems to continue even further to the northwest like an approximately horizontal tunnel. However, this possible extension is not fully reproduced in the 3D model due to the debris cone and dark conditions. The depth of the exposed sinkhole reaches 7 m in the centre, and it is ~2.2 m wide on average. The length of the lower part of the sinkhole (tunnel) reaches at least ~3.5 m, and the width is ~2.5 m. The minimum total volume of the sinkhole is ~45 m^3.

Electrical resistivity tomography

The obtained ERT models clearly show several layers with different electrical resistivities (Fig. 5). Throughout the surveyed area, a layer up to 5 m thick can be seen directly below the ground surface. The thickness of this layer is not uniform across the surveyed profiles (Fig. 5). The resistivity of this layer, for the most part, is close to 10 Ohm.m in resistivity models with 2 m electrode spacing (Fig. 5B, C). The

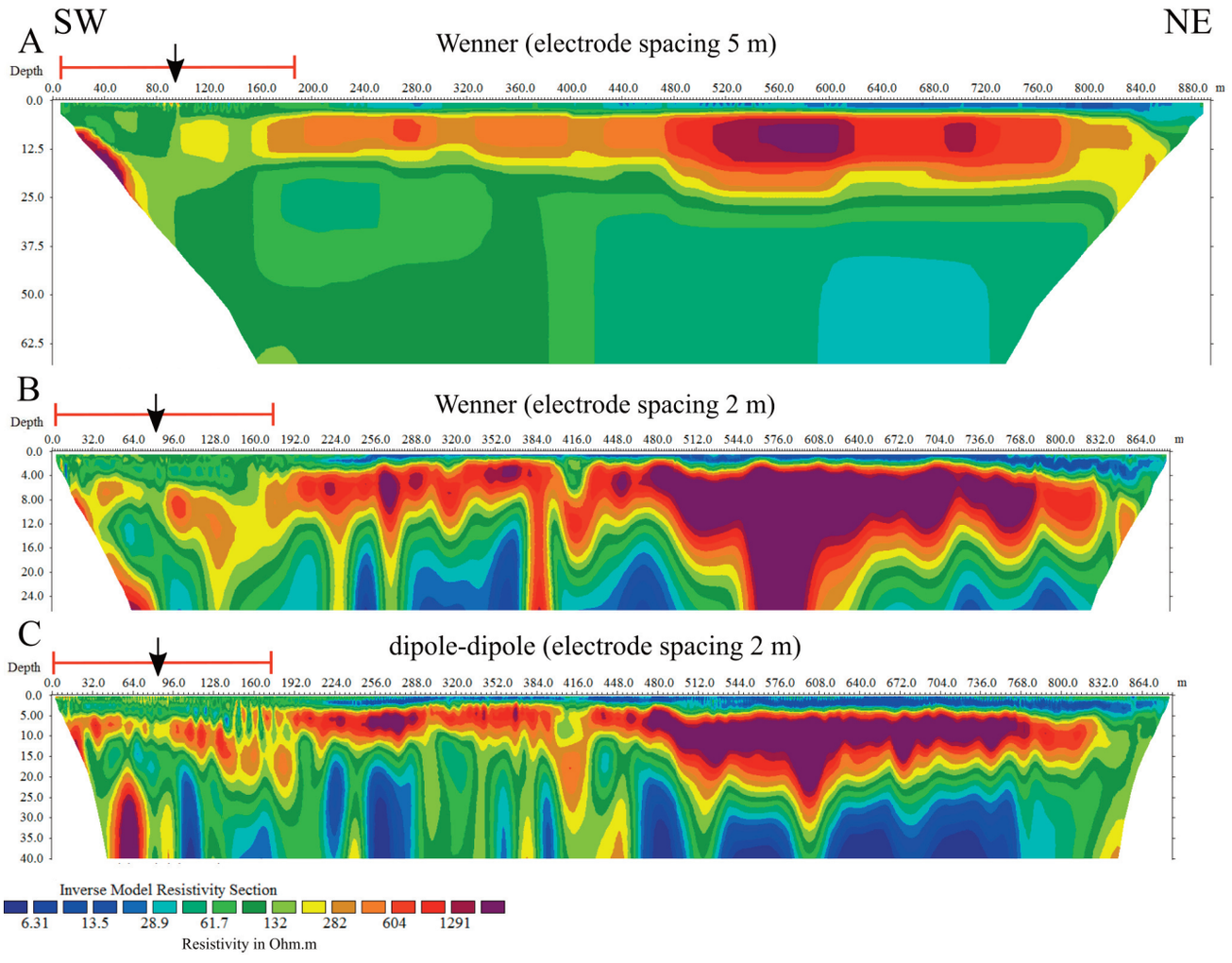

Fig. 5. Resistivity models of the whole survey line. See the location in Fig. 1. Black arrows indicate the site of the karst sinkhole. Note the variable depth of the survey in each profile. In the ERT models, the depth intervals 0–5, 5–17 and 17–60 m correspond to the Quaternary cover, the gypsum of the Salaspils Fm and the clay-rich part of the Salaspils Fm, respectively.

exception is the southwest end of the model, where the karst sinkhole is located. In this part, the resistivity of the uppermost layer is close to 150 Ohm.m (Fig. 6). In a model with 5 m electrode spacing, the resistivity of the uppermost layer is a few tens of Ohm.m higher. We explain the difference in electrical resistivity between the resistivity models with different resolutions for 5 m and 2 m spacing. As the profiles with 2 m spacing have higher resolution and the results are less influenced by the underlying high-resistivity layer than in the case of 5 m spacing, we assume that they provide a more correct assessment of the resistivity of the upper layer. We interpret this layer as glacial till with sand, as it was detected in the sinkhole. The observed resistivity of this layer is slightly less than the range of resistivities reported for typical glacial till (80–2000 Ohm.m; Palacky 1987). Variations in the moisture content could explain the changes in resistivity values across this layer.

At a depth of ~5 m, a second ~12 m thick layer with a resistivity of around 1300 Ohm.m is visible (Fig. 5). In all the obtained profiles, it can be seen that this layer is relatively uniform in the northeastern part, while in the southwestern part, the resistivity of this layer drops to ~1000 Ohm.m, and the layer is also thinner (~7 m). In a 5 m electrode spacing profile, the high-resistivity layer can hardly be traced in the southwestern part of the profile (Fig. 5A). The observed resistivity values fall within the range of resistivities typically reported for carbonate rocks (limestones or dolomites; Reynolds 1997). Guinea et al. (2010) conducted several laboratory tests to conclude that pure gypsum could also be characterised by a resistivity close to 1000 Ohm.m. In our case, the observations in the karst sinkhole suggest that a layer of dolomite should be present in the study area (Fig. 4). This is also expected due to the presence of such a layer in the historical borehole data. The obtained ERT model ends next to the currently active gypsum quarry. There, the Salaspils Fm is 10–15 m thick (Brangulis et al. 1998), approximately the same thickness as the high-resistivity layer (Fig. 5). Combining all available data, we interpret the high-resistivity layer as the Salaspils Fm comprising the gypsum rock.

Below the high-resistivity layer, a relatively uniform resistivity pattern (resistivity values close to 60 Ohm.m) can be seen in the 5 m electrode spacing ERT model (Fig. 5A). ERT models with 2 m electrode spacing show somewhat patchier results. Still, we attribute this to the different resolutions between the profiles. It should be noted that the high-resolution profiles (Fig. 5B, C) show lower resistivity

values for the deepest parts of the profiles than the low-resolution profile (Fig. 5A). Relatively fewer data points could explain this for high-resolution profiles in such a depth. We interpret the drop in resistivity below 20 m depth as an indicator of increased clay content observed in the lower part of the Salaspils Fm (Fig. 2A).

None of the profiles recorded with 2 m electrode spacing show any evidence of a virtually non-conducting object (air-filled void; Fig. 6). In the profile that was recorded with 1 m spacing, only slight variations in resistivity across the actual sinkhole can be seen, indicating some local anomaly (Fig. 6D). It is also apparent that directly below the karst sinkhole, a local zone of high resistivity is present (Fig. 6D). It is hard to judge whether this anomaly is related to a karst sinkhole or an underlying high-resistivity layer that is evident also in profiles with 2 m electrode spacing.

Synthetic modelling

The results of the 2D synthetic modelling of the observed karst sinkhole (Fig. 7A) clearly show that in the 2D case, when 2 m electrode separation is used, the depth of the boundary between the modelled glacial till layer and the clay-rich carbonate layer as well as their respective resistivities can be reconstructed (Fig. 7B, C). Some low-resistivity artefacts are caused by the inversion process close to the karst sinkhole, especially when the dipole-dipole configuration is used (Fig. 7C). Nevertheless, they do not affect the possibilities of karst sinkhole identification. Even when 5 m electrode separation was used (Fig. 7D), 2D modelling suggests that a karst sinkhole of this size will cause a significant resistivity anomaly.

During 3D modelling, the same resistivity model parameters and karst sinkhole shape were used as in 2D modelling. Two ERT profile lines were modelled using the Wenner and dipole-dipole configurations (Fig. 8A).

In Profiles 1 and 2, the depth of the boundary between the layers, as well as their respective resistivities, can be easily reconstructed (Fig. 8B–E). Almost no indication of a karst sinkhole can be seen in the modelled Profile 2. Only when the dipole-dipole configuration is used, a slight in-

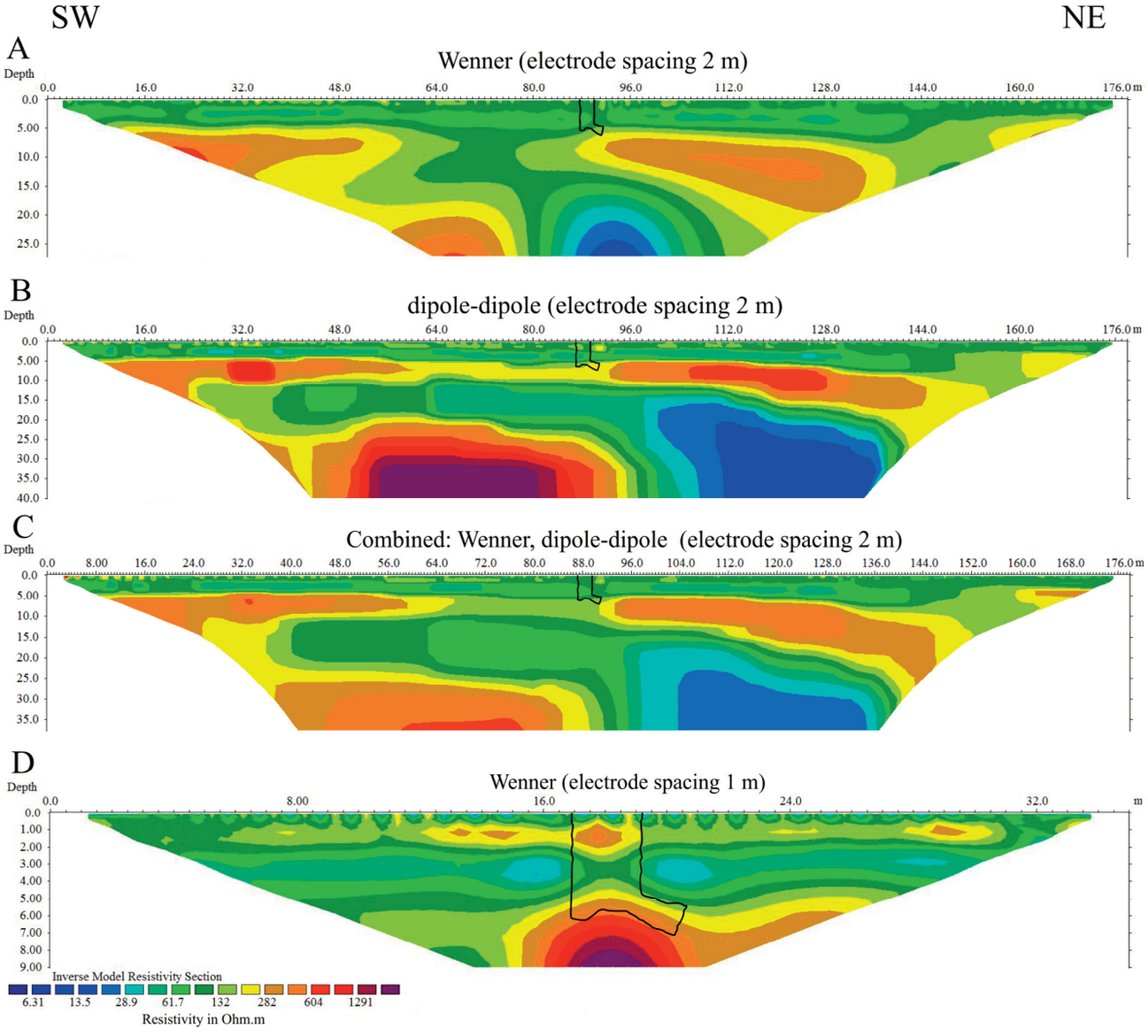

Fig. 6. Close-up of ERT models around the karst sinkhole (marked by black contour). In the ERT models, the depth intervals 0–5, 5–10 m correspond to the Quaternary cover and gypsum of the Salaspils Fm.

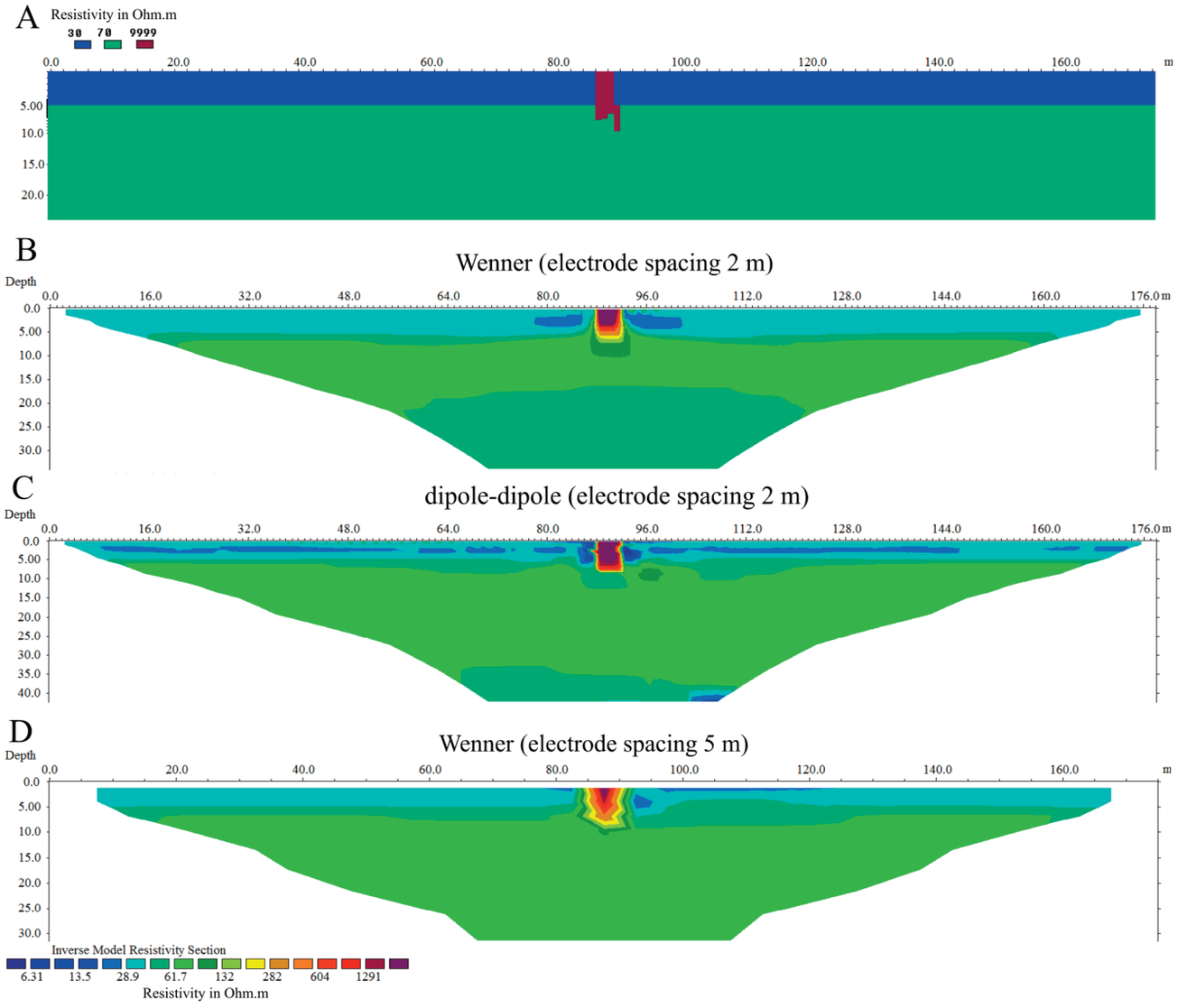

Fig. 7. Results of 2D ERT synthetic modelling. **A** – resistivity model that was used in the modelling process. **B–D** – results obtained for various electrode configurations and electrode spacings.

crease in resistivity is evident right at the top of the sinkhole (Fig 8E). A few more promising results can be seen when the ERT profile is placed directly above the karst sinkhole (Fig. 8B, C). A slight resistivity increase at the top of the sinkhole is visible in the case modelled with the Wenner electrode configuration. In contrast, such a higher resistivity anomaly is more pronounced in the profile modelled with the dipole-dipole configuration. It should be noted that the data obtained during 3D modelling did not show any prominent resistivity anomaly. The modelled data resistivity value of the identified anomaly reached approximately 70 Ohm.m (Fig. 8). Also, no artificial noise was added to the data set, which would only deteriorate the possibilities of identifying such a slight increase in resistivity.

Discussion

Development of the karst sinkhole in the surveyed area

The newly developed sinkhole can be classified as a karst cover-collapse sinkhole. It developed due to the dissolution of the Salaspils Fm gypsum rocks and after the collapse of the overlying deposits of the Daugava Fm (dolomites, dolomitic marls) and Quaternary deposits (glacial till, sands and technogenic deposits). As seen in the 3D model of the sinkhole (Fig. 4), the upper part of the Daugava Fm consists of a rigid slab of dolomite that could resist the overburden pressure of the overlying deposits for some time, allowing the formation (dissolution) of the subsurface void. The possible existence of old (palaeo) karst in the dolomites of the Daugava Fm cannot be excluded. Buried palaeo-karst sinkholes filled with younger Devonian rocks (clays, sandstones) are commonly encountered in the dolomite quarries of the Daugava Fm (Hodireva 1997; Kuršs and Stinkule 1997). However, the most probable mechanism of the sinkhole formation should be related to modern dissolution processes of evaporate rocks (gypsum) of the Salaspils Fm, which are characterised by a high solubility reaching 14 cm per year in the vicinity of Salaspils (Prols et al. 1997). It is known from the literature (Dreybrodt et al. 2002) that gypsum's solubility can reach even 1.8 m per year under speedy water flow. It should be noted that the high water flow could have been

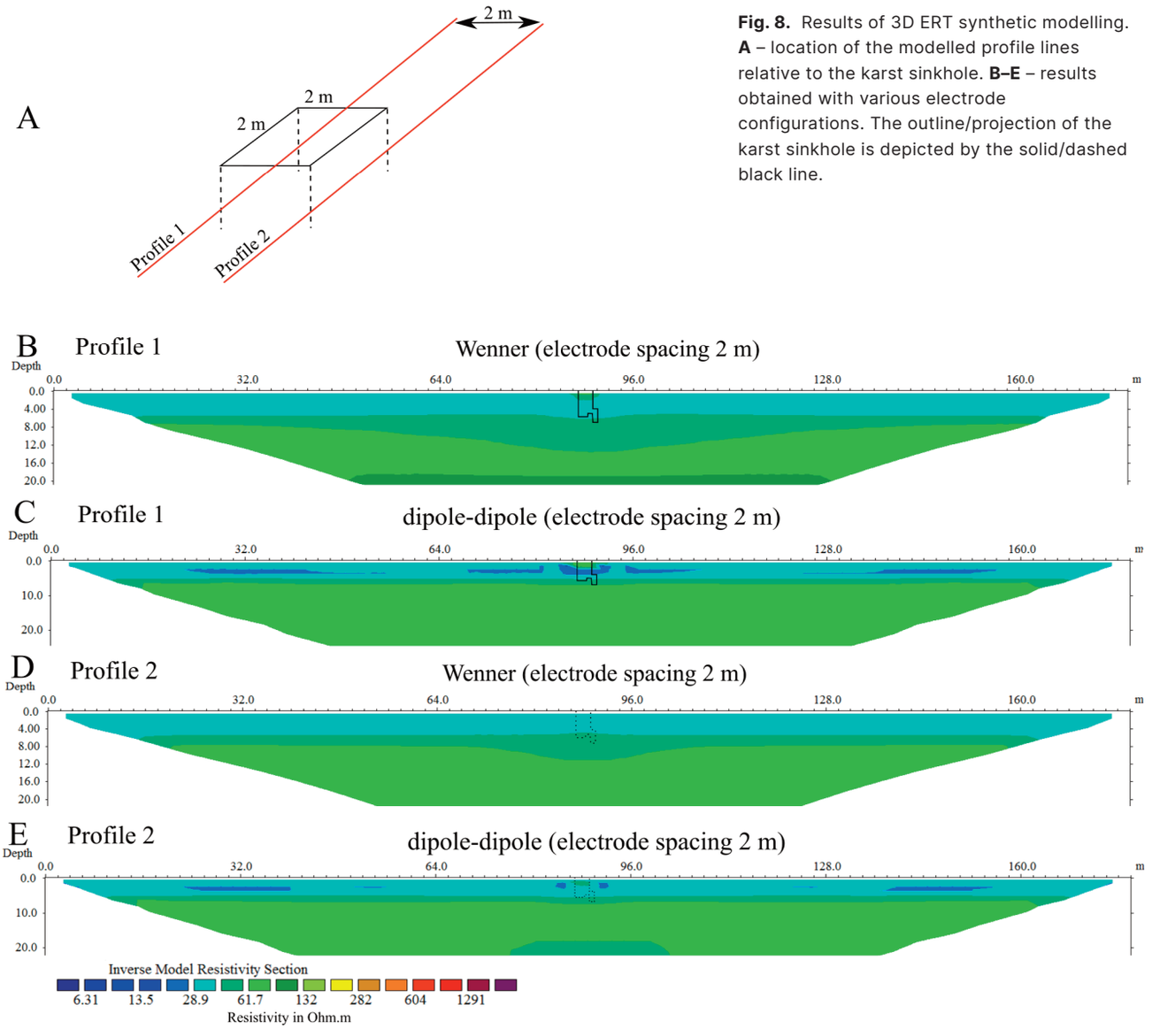

Fig. 8. Results of 3D ERT synthetic modelling. **A** – location of the modelled profile lines relative to the karst sinkhole. **B–E** – results obtained with various electrode configurations. The outline/projection of the karst sinkhole is depicted by the solid/dashed black line.

generated in the vicinity of the Salaspils gypsum quarry due to the lowering of the groundwater table, as described below.

According to Švēde (2001), groundwaters in the aquifer of the Salaspils Fm are saturated with 1.2–1.4 g/L of sulphate ions (SO_4^{2-}). Thus, further dissolution of gypsum is hindered. The only possibility for the activation of karst processes is the input of water which is not saturated with sulphate ions. As the groundwater table at the nearby Salaspils gypsum quarry declined by more than 20 m due to excavation, it created a hydrological depression (dropdown of the water table) in the surroundings. The anthropogenic lowering of the groundwater level supposedly created a thicker vadose zone, facilitating the inflow of surface waters (unsaturated with sulphate ions) into the aquifer of the Salaspils Fm and causing the rapid increase in gypsum dissolution and further enlargement of the karst void.

Application of ERT for the detection of karst sinkholes

The ERT method has been outlined as valuable and cost-effective in karst sinkhole detection (McGrath et al. 2002; El-Qady et al. 2005; Tuckwell et al. 2008; Martínez-Moreno et al. 2014; Brook 2019). However, some studies mention difficulties in identifying subsurface karst features (Sevil et al. 2017).

We obtained data that clearly show several issues that can be encountered if the ERT method is used to identify karst voids. Usually, such detection problems associated with the ERT method are addressed by varying resistivity contrast between a sinkhole and surrounding rocks (Chalikakis et al. 2011). Karst voids can be filled with air, while other parts can be water-filled. Such varying resistivity contrast, in most cases, will result in the opposite resistivity anomaly, which leads to ambiguous interpretation. Festa et al. (2016) noted that if surrounding rocks have a high resistivity, it is hard to detect karst sinkholes. Kaufmann et al. (2011) draw similar conclusions regarding karst sinkholes in limestones or dolostones, as both of those rocks have resistivities of ~2000 Ohm.m. Martínez-Moreno et al. (2015) highlight the same problem with air-filled caves in gypsum. In our study, the karst sinkhole is only partly enclosed by rocks with a high electrical resistivity (1000 Ohm.m). The upper part of the sinkhole is enclosed by a glacial till with a resistivity close to 100 Ohm.m (Figs 4 and 6). Thus, our results show that problems in detecting karst sinkholes can arise in areas where surrounding

rocks have a relatively high resistivity and in areas where surrounding rocks have a relatively low resistivity.

Chalikakis et al. (2011) concluded that despite their near-infinite resistivity, the detection of air-filled karst voids still depends on their volume and depth. The results of this study show that even when a karst void (in this case represented as an open sinkhole) has a diameter twice larger than the minimum electrode spacing and is directly below the ground surface, it can still remain undetected by ERT surveys. It should be emphasised that the ERT profiles in this study were located above the overhanging part (which later collapsed) of the 7-m-deep sinkhole. Thus, our study raises important questions related to the limitations of the ERT method used for detecting karst voids of small and medium dimensions. The applied aspect of our work underlines the importance of the ERT survey grid, which should be very densely spaced if detecting all karst voids is the primary aim of the study. In our case, even the ERT profiles with an electrode spacing of 1 m and located above the overhanging part of the recent sinkhole allowed the detection of only slight variations of the resistivity across the actual sinkhole. Even this anomaly may be related to an underlying high resistivity layer, not the sinkhole itself. We also emphasise that the ERT profiles with an electrode spacing of 2 m and larger did not allow the detection of an open sinkhole with the average minimum dimensions of 2.2 × 7.0 m.

Al-Hameedawi et al. (2021), using modelling techniques, showed that a near-surface low-resistivity layer, as well as near-surface inhomogeneities, can significantly deteriorate data quality, especially if dipole-dipole configuration is used in ERT surveys. In this study, the ERT profile was placed on a gravel/construction debris road that most likely created some near-surface resistivity inhomogeneities. This could explain why there is a notable difference between the data obtained with different electrode configurations (Figs 5 and 6). The results obtained with the dipole-dipole configuration produce a rather patchy structure at some parts of the profile that is consistent with other surveys (e.g., Al-Hameedawi et al. 2021). Zhou et al. (2002) concluded that the dipole-dipole array is the most suitable electrode configuration for detecting sinkholes and argued that the Wenner configuration should not be used. He also noted that if Wenner and dipole-dipole configurations are applied simultaneously, the results resemble those of dipole-dipole. Similarly, El-Qady et al. (2005) outline the dipole-dipole configuration as the most suitable for mapping cavities. In this study, the obtained data show similar patterns. Nonetheless, despite locating the ERT profiles above the overhanging part of the karst sinkhole, we were not able to detect the karst sinkhole regardless of the applied electrode configuration.

We also found that the data obtained by 2D modelling are misleading. While 2D modelled data were used, it seemed that it should be possible to locate a karst sinkhole of the same size as the sinkhole in our survey area. In the modelled data, a clear resistivity anomaly was visible even when 5 m electrode separation was applied (Fig. 7). This result strongly contradicts the actual data that we gathered in the field, where it was impossible to detect high-resistivity anomaly at all, regardless of the electrode configuration (Fig. 6). Satitpittakul et al. (2013) showed that the location of the 2D ERT profile relative to the karst sinkhole can play a major role in the determination of its size and depth. He emphasised the edge effect as a major source of errors. We demonstrate that a still voluminous air-filled karst sinkhole can be missed altogether (Fig. 6D). We attribute this to the 3D effect – our surveyed karst sinkhole can be considered a local high-resistivity zone located in much more conductive surrounding rocks. As a result, an electrical current tends to flow around the karst sinkhole, which is not visible in the obtained data. This interpretation is supported by our 3D modelling results (Fig. 8). A similar conclusion was drawn by Satitpittakul et al. (2013), who highlighted that due to the 3D effect, it is possible that in specific cases where the ERT profile lies directly above a known cavity, there is no high-resistivity anomaly or one that is smaller than the actual size of the cavity. It is doubtful that additional ERT profiles oriented perpendicular to those recorded in this study would change the outcome, as the 3D effect will still be an issue. This study demonstrates that 2D modelling should not be used to assess the possibilities of identifying local structures. Reliable assessment results can only be achieved using 3D modelling techniques.

Conclusions

Our study describes the newly developed karst-cover sinkhole associated with highly soluble gypsum rocks. It demonstrates the limitations of ERT surveys with variable electrode configurations and spacings between electrodes for identifying such karst features.

We have established that limitations in detecting air-filled karst voids can arise in areas where surrounding rocks have a high electrical resistivity and where surrounding rocks have a low resistivity. Using variable spacings between electrodes, we have demonstrated that a newly developed sinkhole in low-resistivity surrounding rocks remains undetectable by ERT due to the 3D effect, even if the ERT profiles are placed directly above the overhanging part of the sinkhole. This issue cannot be overlooked when the ERT method is used to detect subsurface cavities in construction sites.

This study emphasises that assessing the possibilities of identifying subsurface cavities with the ERT method cannot really be conducted using 2D synthetic modelling. Instead, reliable assessment results can only be achieved using 3D synthetic modelling techniques. We also accentuate the need for further detailed investigations of karst processes in Latvia, which have not been adequately surveyed and monitored so far, despite being critical for urban planning and environmental risk assessment.

Acknowledgements

This research was funded by the University of Latvia grant No. AAp2016/B041//Zd2016/AZ03 project ‘Climate change and sustainable use of natural resources’ and project ‘Strengthening of the capacity of doctoral studies at the University of Latvia within the framework of the new doctoral model’, identification No. 8.2.2.0/20/I/006. We thank Jüri Plado and

an anonymous reviewer for the constructive comments and corrections that improved the quality of the manuscript. The publication costs of this article were covered by the Estonian Academy of Sciences.

References

Agisoft. 2021. *Agisoft Metashape User Manual: Professional Edition, Version 1.7*.

Al-Hameedawi, M. M., Thabit, J. M. and Al-Menshed, F. H. 2021. Some notes about three types of inhomogeneity and their effect on the electrical resistivity tomography data. *Journal of Applied Geophysics*, **191**, 104360.

Brangulis, A. J., Kuršs, V., Misāns, J. and Stinkulis, Ģ. 1998. Latvijas ģeoloģija: 1:500 000 mēroga ģeoloģiskā karte un pirmskvartāra nogulumu apraksts (Geology of Latvia: Geological map in scale 1:500 000 and description of bedrock). State Geological Survey, Riga.

Brook, M. S. 2019. Engineering geophysics and the 2017 New Zealand Ground Investigation Specification guidelines. *Engineering Geology*, **252**, 164–167.

Chalikakis, K., Plagnes, V., Guerin, R., Valois, R. and Bosch, F. P. 2011. Contribution of geophysical methods to karst-system exploration: an overview. *Hydrogeology Journal*, **19**, 1169–1180.

Drahor, M. G. 2019. Identification of gypsum karstification using an electrical resistivity tomography technique: The case-study of the Sivas gypsum karst area (Turkey). *Engineering Geology*, **252**, 78–98.

Dreybrodt, W., Romanov, D. and Gabrovsek, F. 2002. Karstification below dam sites: a model of increasing leakage from reservoirs. *Environmental Geology*, **42**(5), 518–524.

Džeriņš, P., Karušs, J., Lamsters, K., Ješkins, J. and Ķelpe, A. 2023. Investigation of buried karst sinkholes under a bog using ground penetrating radar (GPR) and electrical resistivity tomography (ERT). *Earth Surface Processes and Landforms*, **48**(10), 1909– 1925.

El-Qady, G., Hafez, M., Abdalla, M. A. and Ushijima, K. 2005. Imaging subsurface cavities using geoelectric tomography and ground-penetrating radar. *Journal of Cave and Karst Studies*, **67**(3), 174–181.

Festa, V., Tripaldi, S., Siniscalchi, A., Acquafredda, P., Fiore, A., Mele, D. and Romano, G. 2016. Geoelectrical resistivity variations and lithological composition in coastal gypsum rocks: A case study from the Lesina Marina area (Apulia, southern Italy). *Engineering Geology*, **202**, 163–175.

Ford, D. and Williams, P. 2007. *Karst Hydrogeology and Geomorphology*. John Wiley & Sons, Hoboken, NJ.

Geotomo Software. 2017. *User manual: Rapid 2-D Resistivity & IP inversion using the least-squares method.*

Gökkaya, E., Gutiérrez, F., Ferk, M. and Görüm, T. 2021. Sinkhole development in the Sivas gypsum karst, Turkey. *Geomorphology*, **386**, 107746.

Guinea, A., Playa, E., Rivero, L., Himi, M. and Bosch, R. 2010. Geoelectrical classification of gypsum rocks. *Surveys in Geophysics*, **31**(6), 557–580.

Gutiérrez, F., Cooper, A. H. and Johnson, K. S. 2008. Identification, prediction, and mitigation of sinkhole hazards in evaporite karst areas. *Environmental Geology*, **53**(5), 1007–1022.

Gutiérrez, F., Parise, M., De Waele, J. and Jourde, H. 2014. A review on natural and human-induced geohazards and impacts in karst. *Earth-Science Reviews*, **138**, 61–88.

Hodireva, V. 1997. *Latvijas dolomītu litoloģiski rūpnieciskie tipi* (*Lithological industrial types of Latvian Devonian dolomites*). PhD thesis. University of Latvia.

Ivanova, O. and Nulle, I. 2002. Kristāliskā pamatklintāja virsmas strukturālā karte. Mērogs 1:500 000 (Top crystalline basement depth structural map. Scale 1:500 000). In *Latvijas tektonika* (*Tectonics of Latvia*) (Brangulis, A. J. and Kaņevs, S., eds). State Geological Survey, Riga.

Karušs, J., Lamsters, K., Poršņovs, D., Zandersons, V. and Ješkins, J. 2021. Geophysical mapping of residual pollution at the remediated Inčukalns acid tar lagoon, Latvia. *Estonian Journal of Earth Sciences*, **70**(3), 140–151.

Kaufmann, G., Romanov, D. and Nielbock, R. 2011. Cave detection using multiple geophysical methods: Unicorn cave, Harz Mountains, Germany. *Geophysics*, **76**(3), B71–B77.

Kuršs, V. and Stinkule, A. 1997. *Latvijas derīgie izrakteņi* (*Mineral Deposits of Latvia*). University of Latvia, Riga.

Lamsters, K., 2012. Drumlins and related glaciogenic landforms of the Madliena Tilted Plain, Central Latvian Lowland. *Bulletin of the Geological Society of Finland*, **84**(1), 45–57.

Lamsters, K. and Zelčs, V. 2015. Subglacial bedforms of the Zemgale Ice Lobe, south-eastern Baltic. *Quaternary International*, **386**, 42–54.

Lamsters, K., Kalińska-Nartiša, E., Zelčs, V. and Alexanderson, H. 2017. New luminescence ages reveal Early to Middle Weichselian deposits in central Latvia. *Geological Quarterly*, **61**(2), 480–490.

Lamsters, K., Karušs, J., Stūrmane, A., Ješkins, J. and Džeriņš, P. 2022. Mapping of large-scale diapir structures at the paleo-ice tongue bed in western Latvia from geophysical investigations and borehole data. *Quaternary International*, **630**, 3–16.

LEGMC (Latvian Environment, Geology and Meteorology Centre). 2021. *Meteorological data from station "Riga-University"*. https://videscentrs.lvgmc.lv/ (accessed 2023-01-19).

Levins, I. and Buzajevs, V. 1999. Pazemes ūdeņu aizsargātības karte. Mērogs 1:500 000 (Groundwater vulnerability map of Latvia, scale 1:500 000). Report No. 12074. State Geological Survey, Riga.

Loke, M. H. 2004. *Tutorial: 2-D and 3-D Electrical Imaging Surveys. Geotomo Software*, *Res2dinv 3.5 Software*.

Loke, M. H. and Barker, R. D. 1996. Rapid least-squares inversion of apparent resistivity pseudosections by a quasi-Newton method. *Geophysical Prospecting*, **44**, 131–152.

Martel, R., Castellazzi, P., Gloaguen, E., Trépanier, L. and Garfias, J. 2018. ERT, GPR, InSAR, and tracer tests to characterize karst aquifer systems under urban areas: The case of Quebec City. *Geomorphology*, **310**, 45–56.

Martínez-Moreno, F. J., Galindo-Zaldívar, J., Pedrera, A., Teixido, T., Ruano, P., Peña, J. A. et al. 2014. Integrated geophysical methods for studying the karst system of Gruta de las Maravillas (Aracena, Southwest Spain). *Journal of Applied Geophysics*, **107**, 149–162.

Martínez-Moreno, F. J., Galindo-Zaldívar, J., Pedrera, A., González-Castillo, L., Ruano, P., Calaforra, J. M. et al. 2015. Detecting gypsum caves with microgravity and ERT under soil water content variations (Sorbas, SE Spain). *Engineering Geology*, **193**, 38–48.

McGrath, R. J., Styles, P., Thomas, E. and Neale, S. 2002. Integrated high-resolution geophysical investigations as potential tools for water resource investigations in karst terrain. *Environmental Geology*, **42**, 552–557.

Palacky, G. V. 1987. Resistivity characteristics of geologic targets. In *Electromagnetic Methods in Applied Geophysics – Theory* (Nabighian, M., ed.). Society of Exploration Geophysicists, Tulsa, OK, **1**, 53–129.

Pando, L., Pulgar, J. A. and Gutiérrez-Claverol, M. 2013. A case of man-induced ground subsidence and building settlement related to karstified gypsum (Oviedo, NW Spain). *Environmental Earth Sciences*, **68**, 507–519.

Paukstys, B. and Narbutas, V. 1996. Gypsum karst of the Baltic Republics. *International Journal of Speleology*, **25**(3), 279–284.

Prols, J., Driķis, V. and Levins, G. 1997. Vides aizsardzības pasākumu programma Rīgas ģipšakmens atradnes Salaspils iecirkņa izstrādei (Program of environmental protection measures for the development of the Salaspils precinct of Riga gypsum deposit). Latģeo report. State Geological Fund, Riga.

Rao, Y., Guo, Y. and Xu, D. 2021. Detecting karst voids based on dominant frequencies of seismic profiles. *Pure and Applied Geophysics*, **178**(8), 3057–3067.

Reynolds, J. M. 1997. *An Introduction to Applied and Environmental Geophysics*. Wiley, New York.

Satitpittakul, A., Vachiratienchai, C. and Siripunvaraporn, W. 2013. Factors influencing cavity detection in karst terrain on two-dimensional (2-D) direct current (DC) resistivity survey: A case study from the western part of Thailand. *Engineering Geology*, **152**(1), 162–171.

Sevil, J., Gutiérrez. F., Zarroca, M., Desir, G., Carbonel, D., Guerrero, J. et al. 2017. Sinkhole investigation in an urban area by trenching in combination with GPR, ERT and high-precision leveling. Mantled evaporite karst of Zaragoza city, NE Spain. *Engineering Geology*, **231**, 9–20.

Švēde, A. 2001. Ģeoekoloģisko izpētes darbu atskaite. Objekts: Salaspils ģipšakmens atradne, zemes dzīļu monitoringa sistēmas izveidošana (Report of geo-ecological research works. Object: Salaspils gypsum deposit, development of ground monitoring system). Report No. 12781. Ltd "Ģeo Izpēte". State Geological Survey, Riga.

Tolstovs, J., Tracevska, L., Sičovs, G. 1991. Отчет о результатах радиолокационных и инженерно-геологических работ в районе Саласпилсского месторождения гипса – II этап (Overview of the results of radiolocation and engineering geological works at Salaspils gypsum deposit area, stage II. Riga). No. 10824. State Geological Survey, Riga.

Tuckwell, G., Grossey, T., Owen, S. and Stearns, P. 2008. The use of microgravity to detect small distributed voids and low-density ground. *Quarterly Journal of Engineering Geology and Hydrogeology*, **41**(3), 371–380.

Zhou, W., Beck, B. F. and Adams, A. L. 2002. Effective electrode array in mapping karst hazards in electrical resistivity tomography. *Environmental Geology*, **42**, 922–928.

Kipsikihis paikneva kuiva karstiõõnsuse tuvastatavuse piirangud eritakistustomograafilise uurimismeetodi puhul: näide Balti Devoni settebasseinist

Jānis Karušs, Pēteris Džeriņš, Kristaps Lamsters, Jurijs Ješkins ja Ģirts Stinkulis

Karstinähtustest mõjutatud maastikud on levinud kogu maailmas, põhjustades probleeme ehitiste rajamisele ja püsimisele ning julgeolekule. Kuigi maa-aluste karstinähtuste uurimisel peetakse kõige sobivamaks eritakistuse tomograafilist (ERT) meetodit, mõjutavad lokaalsed geoloogilised tingimused mõõtmistulemuste interpretatsiooni oluliselt. Artikkel kirjeldab Läti Salaspilsi lademe kipsikihtidesse tekkinud karstikoopa ERT uuringuid eesmärgiga analüüsida meetodi piiranguid maapinnalähedaste karstitühemike tuvastamisel. Tulemused näitavad, et hiljuti sisselangenud karstikoobas oli ERT andmetes tuvastamatu, hoolimata profiili paigutumisest vahetult 7 m sügavuse koopa kohale. Vastupidiselt mõõtmistulemustele viitab kahemõõtmeline sünteetiline modelleerimine sellele, et mõõdetuga sarnase suurusega karstikoobas on ERT andmetes kergesti äratuntav. Seevastu kolmemõõtmelise sünteetilise modelleerimise tulemused sarnanevad välitööde andmetele, see tähendab ei viita karstikoopa elektrilisele signaalile. Töö tulemusel järeldatakse, et maa-aluste õõnsuste tuvastamise võimaluste hindamiseks peaks kasutama kolmemõõtmelise sünteetilise modelleerimise abi. Töö tulemused näitavad ka seda, et kuivade karstikoobaste tuvastamise probleemid ERT meetodi abil võivad tekkida mitte ainult seal, kus karstinähtust sisaldavatel kivimitel on kõrge eritakistus, vaid ka seal, kus kivimid on madala takistusega.